

Cholesterol Depletion Induces Solid-like Regions in the Plasma Membrane

Stefanie Y. Nishimura,* Marija Vrljic,[†] Lawrence O. Klein,[‡] Harden M. McConnell,^{*‡} and W. E. Moerner^{*‡}

*Department of Chemistry, [†]Molecular and Cellular Physiology, and [‡]Biophysics Program, Stanford University, Stanford, California 94305-5080

ABSTRACT Glycosylphosphatidylinositol-linked and transmembrane major histocompatibility complex (MHC) class II I-E^k proteins, as well as *N*-(6-tetramethylrhodaminethiocarbonyl)-1,2-dihexadecanoyl-*sn*-glycero-3-phosphoethanolamine (Tritc-DHPE), are used as probes to determine the effect of cholesterol concentration on the organization of the plasma membrane at temperatures in the range 22°C–42°C. Cholesterol depletion caused a decrease in the diffusion coefficients for the MHC II proteins and also for a slow fraction of the Tritc-DHPE population. At 37°C, reduction of the total cell cholesterol concentration results in a smaller suppression of the translational diffusion for I-E^k proteins (twofold) than was observed in earlier work at 22°C (five sevenfold) Vrljic, M., S. Y. Nishimura, W. E. Moerner, and H. M. McConnell. 2005. *Biophys. J.* 88:334–347. At 37°C, the diffusion of both I-E^k proteins is Brownian ($0.9 < \alpha$ -parameter < 1.1). More than 99% of the protein population diffuses homogeneously when imaged at 65 frames per s. As the temperature is raised from 22°C to 42°C, a change in activation energy is seen at ~35°C in the Arrhenius plots. Cytoskeletal effects appear to be minimal. These results are consistent with a previously described model of solid-like domain formation in the plasma membrane.

INTRODUCTION

There is much interest in the relation between lipid organization found in model membranes and proposals for the lipid organization in cell membranes. The plasma membrane differs from most model membranes in that it has an asymmetric lipid composition, a greater diversity of lipids, a high concentration of proteins, cytoskeletal elements, and membrane trafficking processes. The roles of these different factors in determining lipid organization are under investigation in many laboratories.

In model systems, such as lipid monolayers and bilayers, liquid-liquid immiscibility for certain mixtures of lipids has been observed using fluorescence microscopy (1–5). Liquid-liquid immiscibility has been observed for a number of lipid compositions and always depends on the presence of cholesterol. For example, vesicles composed of certain lipid ternary mixtures show liquid-liquid immiscibility. Cholesterol depletion using β -cyclodextrin (β -CD) changes the relative proportion of the two coexisting phases (6). The absence of cholesterol, or its depletion, can also be related to a solid phase in these systems (6–9).

The size and shape of lipid domains observed in model systems depends on composition, temperature, and pressure. Lipid domains can be as large as 10 microns in diameter (6–9). Deuterium NMR line broadening has been interpreted as being due to domains as small as several nanometers (10,11). Molecular complexes termed “condensed complexes” between cholesterol and certain phospholipids have been described (12–14). Condensed complexes may be present in a concentrated separate phase or as a homogeneous mixture with excess phospholipid or cholesterol (15,16).

Lipid-mediated structures are thought to exist in cell membranes, but consensus has not been reached on whether they are related to a thermodynamic phase separation. A true phase separation has not been detected in plasma membranes (however, see Hao et al. (28)), although lipids extracted from these membranes have been shown to exhibit phase separation when reconstituted into monolayers or bilayers (2,3,17).

Detergent resistance in membrane extracts has been interpreted as evidence of lateral heterogeneity in the plasma membrane, with saturated phospholipids, sphingomyelin, cholesterol, and certain proteins such as GPI-linked proteins associating with the detergent resistant membrane (DRM) fraction (18–21). The interpretation of DRM results is controversial (22). In the absence of detergents, DRM-associated proteins were observed to be homogeneously distributed in the plasma membrane and to cluster with each other or with other DRM components only after cross-linking (23,24).

Various studies have attempted to measure domain sizes in plasma membranes with varying results (25–28). Differences in reported domain sizes could be due to variation in technique, probe selection, cell type, or cholesterol level. These issues have been discussed in several recent reviews (16,27,29,30). What is clear is that cholesterol plays an important role in regulating the viscosity of the plasma membrane, cell signaling, resistance to cross-linking, and the occurrence of DRM fractions (23,31–37).

In this study, we are concerned with the role of cholesterol in plasma membrane organization, with the specific goal of understanding the decrease in the diffusion coefficients of proteins and lipids mediated by cholesterol extraction (26, 35,38,39). To this end we have used single-molecule imaging of fluorescently labeled MHC class II I-E^k membrane-anchored proteins (labeled by binding of a fluorescently labeled antigenic peptide) as well as fluorescent lipid analogs,

Submitted July 11, 2005, and accepted for publication October 14, 2005.

Address reprint requests to Stefanie Y. Nishimura, E-mail: snishimu@stanford.edu.

© 2006 by the Biophysical Society

0006-3495/06/02/927/12 \$2.00

doi: 10.1529/biophysj.105.070524

DiIC₁₈ and *N*-(6-tetramethylrhodaminethiocarbonyl)-1,2-dihexadecanoyl-*sn*-glycero-3-phosphoethanolamine (Tritc-DHPE). Previous analysis found 30–50% of the glycosylphosphatidylinositol (GPI)-linked I-E^k and 5–25% of the transmembrane I-E^k to be localized in the DRM fraction (25). By comparing the observed translational diffusion of these probes to unconstrained Brownian motion, we can distinguish modes of motion such as free diffusion, restricted diffusion, or directed motion. As we then vary the plasma membrane cholesterol concentration and temperature, the resulting changes in the motion of the membrane probes provide clues as to the molecular aspects of translational diffusion in cell membranes.

MATERIALS AND METHODS

Cell culture

Chinese hamster ovary (CHO) cells transfected with either mouse MHC class II protein I-E^k (CHO-I-E^k) or with the I-E^k extracytoplasmic domain fused with a GPI-linker (CHO-GPI-linked I-E^k) were a generous gift from M. M. Davis (40). CHO cells were grown in Roswell Park Memorial Institute (RPMI) 1640 phenol red-free media (Gibco BRL, Grand Island, NY) supplemented with 10% fetal calf serum (FCS; HyClone, Logan, UT), 10 mM HEPES (4-(2-hydroxyethyl)-1-piperazineethanesulfonic acid), 1 mM sodium pyruvate, 20 μM 2-mercaptoethanol (2-hydroxy-1-ethanethiol), and 0.1 mM nonessential amino acids, 0.5 mg/ml geneticin (Gibco BRL), pH 7.4, and 5% carbon dioxide at 37°C. A more detailed description of the cell culture is provided in a previous report (25).

Labeling with Cy5-MCC and Tritc-DHPE; TNBS treatment

For the I-E^k studies, cells were labeled by incubation with 0.05–0.5 mg/ml Cy5-MCC 95-103 peptide for 15–30 min at 37°C. For details, see our previous work (25,26). Cells were labeled with Cy5-MCC before treatment with any drug.

Tritc-DHPE or 1,1'-dioctadecyl-3,3,3',3'-tetramethylindocarbocyanine (DiIC₁₈) (Molecular Probes, Eugene, OR) was stored in chloroform (1 mg/ml, stock). Immediately before use, 1–5 μL of dye stock solution was dried into a film and then reconstituted in 20–100 μL of ethanol. CHO-I-E^k or CHO-GPI-I-E^k cells were incubated with a final concentration of 100 nM–1 μM of Tritc-DHPE or 0.1–1 nM DiIC₁₈ for 5–10 min at 22°C in supplemented RPMI 1640 media with FCS. The maximum concentration of ethanol during incubation was 1% v/v. Cholesterol-depleted cells were labeled after treatment with 2 h β-CD, but for all other conditions cells were labeled before the treatment.

2,4,6-trinitrobenzenesulfonic acid (TNBS) was obtained from Sigma (St. Louis, MO). For quenching experiments, cells were first labeled with dye, and then treated with 5 mM TNBS (1 M stock in water) in Dulbecco's phosphate-buffered saline (Gibco) at 22°C. Imaging of the cells was completed within 45 min after addition of TNBS. Control cells were also imaged in Dulbecco's PBS. Diffusion coefficients obtained from cells in Dulbecco's PBS were identical to data taken with the cells in supplemented RPMI.

Cholesterol depletion and repletion

For cholesterol depletion, cells were incubated in 10 mM β-CD (Sigma) or 2×10^{-6} moles β-CD/10,000 cells, in supplemented RPMI with FCS at 37°C for the times indicated in the figures. The total cell cholesterol concentration after treatment of the CHO cells for various times with β-CD

was determined using the Amplex Red Cholesterol Assay (Molecular Probes), and the results were reported in previous work (26). After the times indicated in the figures, the β-CD solution was rinsed and cells were imaged in media without β-CD. For details, see Vrljic et al. (25,26).

Long-term viability of β-CD-treated cells was not affected. At 24 h after β-CD treatment, the cell morphology resembled that of untreated cells and cells were dividing (data not shown). As reported previously, a small fraction of the cells (<10%) exhibited signs of late apoptosis after β-CD treatment, and these cells were excluded from the analysis (26). For additional detail, see Supplementary Material.

Cholesterol was added to the cells using cholesterol-loaded methyl-β-CD (chol-mβ-CD) (Sigma) at 1 mM cholesterol (0.2×10^{-6} moles of cholesterol/10,000 cells). Chol-mβ-CD was dissolved in supplemented RPMI 1640 with 10% FCS, and the cells were incubated at 37°C for the times indicated in the figures. The cholesterol solution was refreshed every 30 min. For the cholesterol repletion studies, cells were first incubated with 10 mM β-CD for 60 or 90 min and then incubated with chol-mβ-CD. Chol-mβ-CD was not present in the media during imaging. Cholesterol loading did not cause an increase in the number of apoptotic cells and did not restore the morphology of the cells to normal on the timescale of the experiments (3 h) (data not shown). The treated cells remained less elongated and more spherical than the cells at normal cell cholesterol concentration. This suggests that the reversal of the cell signaling process responsible for initial loss of cell adhesion points takes longer than 3 h even in the presence of cholesterol.

Cytoskeletal disruption

Stock solutions of nocodazole (Sigma; 20 mM stock) and cytochalasin D (Sigma; 1 mg/ml stock solution) were prepared in DMSO. Control cells were treated with an equivalent amount of dimethyl sulfoxide (DMSO) alone. For tubulin depolymerization, cells were treated for 30 min at 37°C with 100 μM nocodazole before imaging. To disrupt the actin cytoskeleton, cells were treated with 4, 13, or 40 μM cytochalasin D (25,35,41) and imaged immediately at 37°C. The cells were then imaged at 37°C until they became rounded, indicating extensive cytoskeletal rearrangement (~15–30 min). Cell edges remained smooth and cytoplasm displayed a similar number of vacuoles, indicating that cells are not apoptotic. Both drugs were present in the media during imaging. The effect of these drugs has been described elsewhere (42–44).

Imaging media

Cells were cultured on a chambered coverglass (Nalgene Nunc International, Naperville, IL) and imaged in supplemented RPMI 1640 phenol red-free medium. FCS was excluded from the media during imaging to lower the background fluorescence signal. Data taken with and without FCS in the imaging media were identical (26). An enzymatic oxygen scavenger system was used when imaging Cy5: 1% v/v glucose (Sigma; 500 mg/ml stock), 1% v/v glucose oxidase (Sigma; 5000 U/ml stock), 1% v/v catalase (Sigma; 40,000 U/ml stock), and 0.5% v/v 2-mercaptoethanol (Sigma; 14.3 M stock). Diffusion coefficients taken with and without the enzymatic oxygen scavenger system were identical except that the lifetime of the fluorophore before photobleaching was extended in the presence of oxygen scavengers (Supplementary Material). No oxygen scavengers were present in the media when Tritc-DHPE was imaged. For further details, see Vrljic et al. (25,26).

Single-molecule imaging

The fluorescence imaging of the cells was performed with wide-field epillumination in an area of 8-by-8 μm, using an inverted microscope (Eclipse TE300, Nikon, Burlingame, CA). Laser illumination at 633 (106-1, Spectra-Physics, Mountain View, CA) or 532 nm (GS32-20, Intelite Laser, Genoa, NV) provided an intensity of ~2 kW/cm² at the sample plane. The epifluorescence was collected with a 100× magnification, 1.4 numerical

aperture oil-immersion objective (PlanApo, Nikon) and infinity-corrected objective adaptor (Nikon). A 645 nm dichroic mirror and 640 nm ALPHA-Epsilon long-pass filter (Omega Optical, Brattleboro, VT) or a 545 nm dichroic mirror and 540 nm long-pass filter (Omega Optical) were used to filter the emission from Cy5 and Tritc-DHPE/DiIC₁₈, respectively. The emission was collected using an on-chip intensified frame-transfer CCD camera (Cascade 512B, Roper Scientific, Trenton, NJ) at a frame rate of 65 Hz. For further details, see Vrljic et al. (25,26).

Temperature control

The temperature of the sample was varied using a homemade heating stage in combination with an objective heating collar (Biopetechs, Butler, PA). The microscope stage was heated above room temperature using resistive heating tape connected through a variable power supply (Variac, Superior Electric, Bristol, CT), and a Petri dish was placed over the 8-well chambered coverglass on the stage to reduce cooling through air currents. The air temperature was determined using a PT-100 thermocouple (Omega) placed under the plastic dish, and for the 37°C measurements, the air temperature was maintained at 37.1°C ± 0.50°C. The temperature of the solution within each well was measured after equilibration for 1 h and found to be 36.4°C ± 1.1°C. In addition, the diffusion coefficient for the I-E^k protein at normal cholesterol concentration was determined each time the sample was imaged, and this value was used as a secondary calibration for the temperature of the sample (data not shown). The temperature of the stage was varied above room temperature from 27°C–42°C.

Data analysis

For a detailed description of the data analysis methods, see Vrljic et al. (25). Single-molecule positional trajectories were mapped by determining the center of the fluorescent spot in each frame by eye with an accuracy of ~39.5 nm (diameter of one pixel). This spatial resolution was sufficient in this experiment since the average displacement of the I-E^k proteins from frame to frame was ~100–300 nm ($\langle r^2 \rangle = 4Dt$, where $\langle r^2 \rangle$ = mean squared radial displacement for a time lag, $D = 0.2$ – $1.0 \mu\text{m}^2/\text{s}$, $t = 15.4$ ms). The average trajectory lengths in this study were ~0.5 s long before photobleaching.

The diffusion coefficients were determined in two ways. In Figs. 2, 3, and 6, the radial displacements from all trajectories for a particular time lag were combined and fitted to the cumulative radial probability distribution function (CDF) for a Brownian diffuser to extract an estimate of the mean diffusion coefficient (see Supplementary Material for the exact number of trajectories and cells used for each case). In this analysis, the individuality of the trajectories was disregarded and the combined distribution of all independent displacements from all trajectories at a specific time lag was analyzed. In determining the diffusion coefficient, the largest time lag was taken to be the last time at which at least 50 displacements contributed to the fit. In Figs. 1 and 7, the diffusion coefficients were averaged over all time lags to obtain a mean diffusion coefficient.

In the diffusion coefficient versus time lag plots, deviation from Brownian motion was characterized by determining the anomalous diffusion parameter, α . For a two-dimensional random walk $\alpha = 1$ and for anomalous diffusion $0 < \alpha < 1$ ($D = D_0 t^{\alpha-1}$; $\langle r^2 \rangle = 4D_0 t^\alpha$, where D is the observed diffusion coefficient and D_0 is the true diffusion coefficient) (45–47).

In Figs. 4 and 5, the mean-squared displacements from an individual single-molecule trajectory were used according to $D = \langle r^2 \rangle / 4t$, with $t = 30.8$ ms. In this method, each single-molecule trajectory was used to calculate an apparent diffusion coefficient, and the distribution of apparent diffusion coefficients for the individual trajectories was constructed to test for heterogeneity from molecule to molecule. The number of displacements were made uniform for all trajectories by clipping the trajectories such that the first N points from each trajectory were included in the analysis ($N = 20$ for I-E^k and DiIC₁₈ and 10 for Tritc-DHPE data). Histograms were normalized by dividing by the total number of trajectories. The expected distribution of apparent diffusion coefficients for a homogeneous popula-

TABLE 1 Diffusion coefficients

Diffusion coefficient ($\mu\text{m}^2/\text{s}$) at 37°C	GPI-linked I-E ^k	Transmembrane I-E ^k
Normal cholesterol	1.1 ± 0.06	0.59 ± 0.04
Reintroduced cholesterol	0.93 ± 0.08*	0.63 ± 0.05 [†]
Reduced cholesterol	0.49 ± 0.03 [‡]	0.34 ± 0.03 [‡]
Nocodazole after cholesterol depletion	0.39 ± 0.02 [§]	0.19 ± 0.02 [§]
Normal cholesterol (22°C)	0.19 ± 5.9 × 10 ⁻³ (22°C)	0.15 ± 3.3 × 10 ⁻³ (22°C)

*1 h β -CD followed by 2 h chol-m β -CD.

[†]90 min β -CD followed by 2 h chol-m β -CD.

[‡]2 h β -CD.

[§]2 h β -CD followed by nocodazole treatment.

tion of diffusers was computed using the arithmetic mean of the diffusion coefficients from the individual trajectories (25,48).

RESULTS

Diffusion is suppressed after cholesterol depletion when imaged at 37°C

To understand the origin of the suppression of diffusion observed for certain membrane molecules upon cholesterol depletion, the diffusion of I-E^k proteins was monitored as the total cell cholesterol concentration was incrementally reduced by incubating the CHO cells with β -CD. The cell cholesterol was thereby gradually reduced to ~50% of normal (26). The cells were then imaged at physiological temperature (37°C) and results compared with the previous data obtained at room temperature (26) to test whether the suppression of protein motion upon cholesterol depletion also occurs at physiological temperature.

As expected, the mean diffusion coefficients of the GPI-linked and transmembrane I-E^k proteins were higher when the cells were imaged at 37°C than when the cells were imaged at 22°C for all cholesterol concentrations (Fig. 1, C and D and Table 1).

Cholesterol-depletion caused a decrease in the mean diffusion coefficients for both the GPI-linked and transmembrane I-E^k proteins when imaged at 37°C. Also, the mean diffusion coefficients for both proteins decrease as the incubation time with β -CD is increased (Fig. 1, A and B), correlating with the decrease in the total cell cholesterol concentration (Fig. 1, C and D). However, the percentage decrease in the mean diffusion coefficients after cholesterol depletion was only twofold when the cells were imaged at 37°C, a smaller change than the five- or sevenfold decrease observed when cells were imaged at 22°C (Fig. 1, C and D).

Diffusion is restored after cholesterol reintroduction when imaged at 37°C

To confirm that the suppression of the diffusion was reversible and due to changes in cholesterol concentration,

cholesterol was reintroduced to the plasma membrane using chol- β -CD. The cells were first treated with β -CD for 60 min (GPI-linked I-E^k) or 90 min (transmembrane I-E^k), and then the cholesterol-depleted cells were incubated with chol- β -CD for 2 h. The cell cholesterol concentration increased from \sim 50% of normal to above 100% of normal using this method (26). After cholesterol reintroduction, the diffusion coefficients for both proteins increased to the value observed under normal cholesterol concentrations (Fig. 2, A and B, and Table 1).

On the timescale of our experiments, the cholesterol-depleted cells were unable to metabolically restore the cell cholesterol concentration (26) or diffusion coefficients to the original values, even after incubation for 2 or 4 h in cholesterol-containing FCS supplemented RPMI media at 37°C (Fig. 2, A and B). After incubation for 2 h in supplemented RPMI media, the total cell cholesterol concentration was \sim 40% of normal (26). The average diffusion coefficient for the GPI-linked I-E^k population after 2 h β -CD followed by 4 h in supplemented RPMI media was found to be $0.70 \pm 0.06 \mu\text{m}^2/\text{s}$. The average diffusion coefficient for the transmembrane I-E^k population after 90 min β -CD followed by 2 h in supplemented RPMI media was found to be $0.40 \pm 0.02 \mu\text{m}^2/\text{s}$.

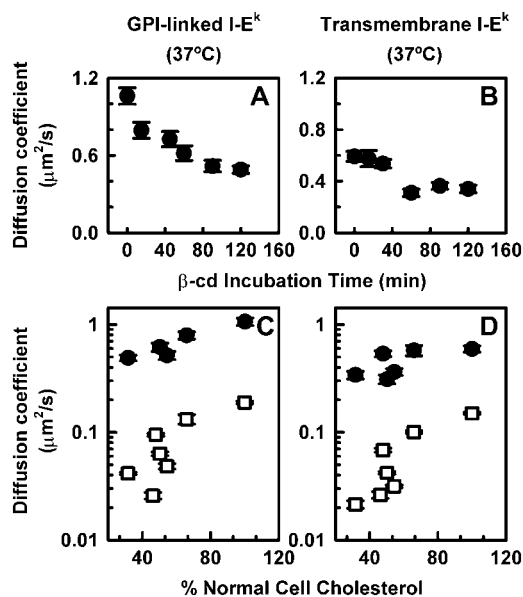


FIGURE 1 Diffusion coefficients after cholesterol depletion. Diffusion coefficients, D , calculated from fits to the cumulative distribution function averaged over all time lags plotted against the corresponding incubation time with β -CD for (A) GPI-linked I-E^k and (B) transmembrane I-E^k. See Fig. 3 for D versus time lags for these data. In all panels, black circles represent data taken at 37°C and white squares represent data taken at 22°C (26). Cholesterol reduction at 22°C results in a fivefold decrease in the D for GPI-linked I-E^k (C) and a sevenfold decrease in the D for transmembrane I-E^k (D) versus an \sim 2-fold decrease at 37°C for both proteins. The percentage normal cell cholesterol concentration as a function of β -CD incubation time has been reported (26). For the number of trajectories contributing to each data point, see Table S1 in the Supplementary Material.

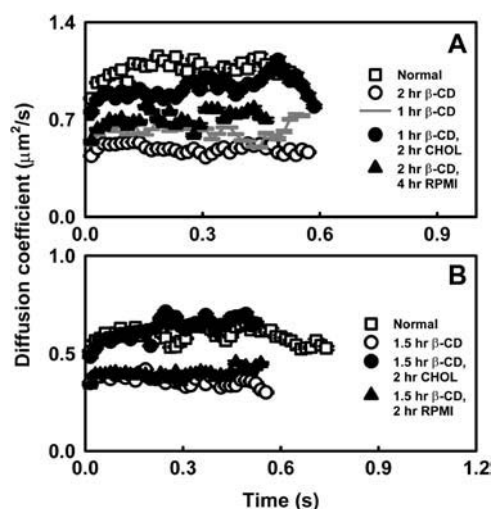


FIGURE 2 Cholesterol reconstitution at 37°C. (A) Diffusion coefficients, D , versus time lag calculated from fits to the cumulative distribution function for GPI-linked I-E^k after cholesterol is reintroduced (B) D versus time lag for transmembrane I-E^k after cholesterol is reintroduced. The diffusion coefficients at normal cholesterol and reduced cholesterol are shown for comparison. The control case (cholesterol depletion followed by incubation in RPMI media) is also shown. The number of trajectories contributing to each data point may be found in the Supplementary Material.

Protein diffusion is predominately Brownian when imaged at 37°C

The diffusion coefficients of GPI-linked and transmembrane I-E^k were examined as a function of time lag from 0.0154 to \sim 0.5 s to determine if the motion of these proteins was constrained at reduced cholesterol concentrations when the cells were imaged at 37°C (Fig. 3, A and B). The α -values for these proteins at room temperature were reported to be between 0.9 and 1.1 (26).

In a few experiments ($<1\%$ of the trajectories), it was apparent that a fluorescent spot was not localized to the plasma membrane, as it either appeared or disappeared as a defocused spot in an area where there were other fluorescent spots in focus. These fluorescent spots then followed a nearly linear trajectory and either moved into or out of focus. These fluorescent spots were clearly located in a focal plane within the cell. Such fluorescent spots included both single molecules of Cy5 that exhibited digital photobleaching and spots that were brighter than expected for a single molecule (data not shown). These fluorescent spots, which exhibited directed motion outside of the plane of the plasma membrane, were not included in the analysis as it was assumed that these molecules were undergoing active transport on cytoskeletal elements. Directed motion was observed at all cholesterol concentrations, but after treatment with a tubulin-disrupting drug (nocodazole), directed motion outside of the plane of the plasma membrane was not observed (data not shown). All molecules were included in the analysis except those above or below the plasma membrane, even if the molecule appeared to be undergoing directed

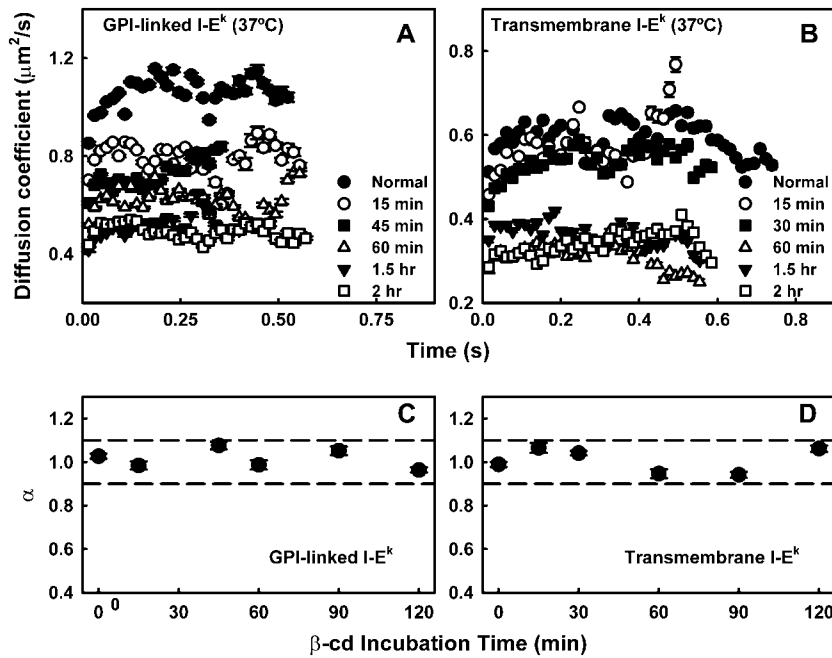


FIGURE 3 Brownian diffusion of proteins at 37°C. Diffusion coefficients at different cholesterol concentrations appear Brownian when measured at 37°C for GPI-linked I-E^k (A) and transmembrane I-E^k (B). The corresponding α -values calculated for the diffusion coefficients at each β -CD incubation time for GPI-linked I-E^k (C) and transmembrane I-E^k (D).

motion. Directed motion outside of the plane of the plasma membrane was not observed in cells imaged at 22°C.

The diffusion coefficients for the GPI-linked and transmembrane I-E^k were found to be predominately Brownian at all cholesterol concentrations when imaged at 37°C. Agreement with Brownian motion was determined by calculating the α -parameter from the diffusion coefficient as a function of time lag plots. The α -values for both the GPI-linked and transmembrane I-E^k, at all observed cholesterol concentrations, were between 0.9 and 1.1, indicating that the motion of the proteins is primarily Brownian for up to ~ 0.5 s (Fig. 3, C and D) and yielding no evidence for confinement.

Protein diffusion is homogeneous

If the I-E^k proteins partitioned into different membrane environments, then heterogeneity in the distribution of diffusion coefficients should be observed. To probe for possible heterogeneity in the protein populations at normal and reduced cholesterol concentrations, histograms were constructed using the apparent diffusion coefficient for each single-molecule positional trajectory at a particular cholesterol concentration (Fig. 4). Individual trajectories were clipped to be 20 steps long (308 ms), and the mean square displacement at time lag 30.8 ms was used to estimate the diffusion coefficient, D_e . The solid line plotted in each histogram is not a fit, but is the expected distribution of measurements for a homogeneous population with a diffusion coefficient given by the mean D_e for each case (48).

At 37°C, the observed distribution of diffusion coefficients for GPI-linked and transmembrane I-E^k for all cholesterol concentrations is described well by a homogeneous

distribution. Reduction in cholesterol concentration caused the entire population of diffusers to shift to a lower diffusion coefficient for both GPI-linked I-E^k (Fig. 4, A–E) and transmembrane I-E^k (Fig. 4, G–K). Upon cholesterol reintroduction, the entire population shifts to a higher average diffusion coefficient (Fig. 4, F and L).

Cholesterol depletion has a varied effect on the diffusion of fluorescent lipid analogs

Histograms of the single-molecule diffusion coefficients for Tritc-DHPE and DiI_{C18} incorporated into the CHO cell plasma membrane at 22°C are shown in Fig. 5. The full distribution of Tritc-DHPE diffusion coefficients is not described well by a homogeneous population of diffusers (Fig. 5, A and B, *solid lines*). For the 22°C data (before and after cholesterol depletion), fits to a two population CDF (49) show that 20% of the Tritc-DHPE had a diffusion coefficient of $\sim 2 \mu\text{m}^2/\text{s}$ and 80% of the population had $D \sim 0.2 \mu\text{m}^2/\text{s}$ (Fig. 5, A and B, *dashed lines*) (25,49). The diffusion coefficient of the faster population did not significantly change after cholesterol depletion, whereas the slower diffusion coefficient decreased by a factor of ~ 6 to a diffusion coefficient of $0.03 \mu\text{m}^2/\text{s}$ (Fig. 5, A and B). When the Tritc-DHPE diffusion coefficients were measured in the presence of a fluorescence quencher (TNBS) with low membrane permeability at 22°C, the relative size of the slower population decreased by 25% (Fig. 5 C). During the time of the experiment, TNBS primarily quenches the fluorescence of Tritc-DHPE and DiI localized in the outer membrane leaflet (Supplementary Material, (50,51)). Cholesterol depletion had no effect on the observed distribution of diffusion coefficients for Tritc-DHPE when TNBS

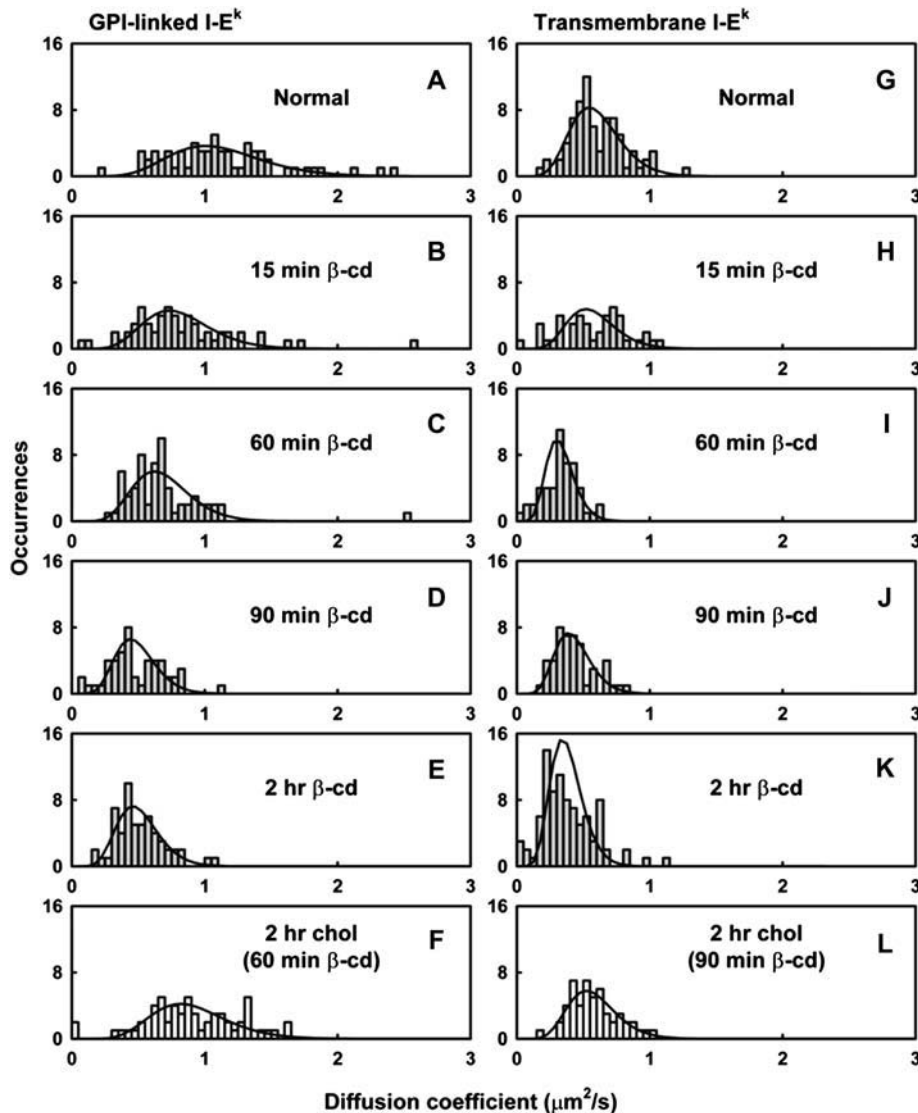


FIGURE 4 Distributions of diffusion coefficients for individual MHC proteins at 37°C. Individual trajectories were clipped to be 20 steps long and a time lag of 30.8 ms was chosen such that 10 displacements from each track were used to calculate each diffusion coefficient. The solid line represents the expected distribution of diffusion coefficients for a homogeneous population of Brownian diffusers (25). The effect of cholesterol depletion on the distribution of D s for GPI-linked I-E^k is depicted in panels A–E and for transmembrane I-E^k in panels G–K. The distributions of D s are shown for GPI-linked I-E^k (F) and for transmembrane I-E^k (L) after cholesterol is reintroduced. See Supplementary Material for the number of tracks used for each histogram.

was present (Fig. 5 D), indicating that diffusion of Tritc-DHPE on the inner leaflet is unaffected by cholesterol depletion. Data for Tritc-DHPE at 37°C are shown in the Supplementary Material.

The distributions of diffusion coefficients for DiC₁₈ before and after cholesterol depletion are shown in Fig. 5, E and F. The DiC₁₈ distributions were predominately homogeneous. The distributions of diffusion coefficients for DiIC₁₈ in the presence of TNBS are shown in Fig. 5, G and H. The mean diffusion coefficient of DiIC₁₈ at the normal cholesterol concentration did not change when TNBS was present during imaging: D (no TNBS) = $1.08 \pm 0.09 \mu\text{m}^2/\text{s}$ and D (with TNBS) = $1.12 \pm 0.06 \mu\text{m}^2/\text{s}$ (one population fit). After cholesterol depletion, the mean of the full DiC₁₈ distribution shifted to $0.69 \pm 0.06 \mu\text{m}^2/\text{s}$ (Fig. 5 F). When TNBS was present, the mean diffusion coefficient for the cholesterol-depleted case was found to be $0.90 \pm 0.11 \mu\text{m}^2/\text{s}$ (Fig. 5 H).

Reduction in mobility is not due to cytoskeletal interactions

Treatment of the cholesterol-depleted cells with cytochalasin D, a drug that prevents actin polymerization, did not restore the mobility of the GPI-linked or transmembrane I-E^k (Fig. 6, A and B). Cholesterol-depleted cells (pretreated with 2 h β-CD) were exposed to 4, 13, or 40 μM cytochalasin D according to several protocols recently reported (26,35,41). The cells were imaged with cytochalasin D present in the media, at 37°C, only until the cells began to look more spherical—a criterion used for cytochalasin D experiments in the Kusumi lab (52). Cell sphericity indicates more extensive actin cytoskeletal rearrangements and loss of actin stress fibers. The mean diffusion coefficients obtained after treatment with each of these three protocols were identical to the 2 h β-CD case.

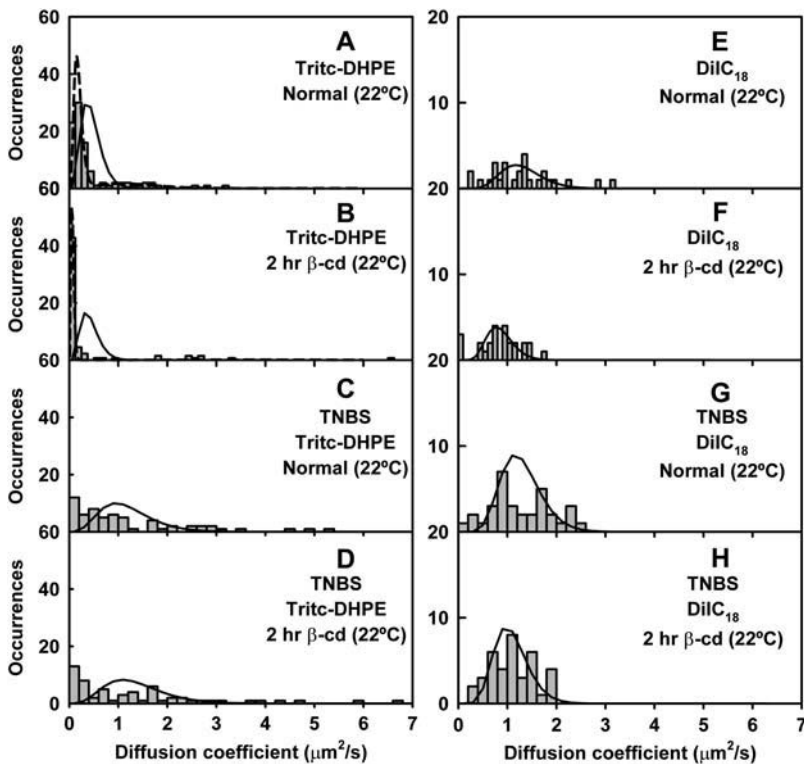


FIGURE 5 Distributions of diffusion coefficients for individual fluorescent lipid analogs. Individual trajectories were clipped to be 10 steps long for Tritc-DHPE and 20 steps for DiIC₁₈. A time lag of 30.8 ms was chosen such that 5 or 10 displacements were used to calculate a diffusion coefficient for each track. The solid lines represent the expected homogeneous distribution of D_s given the average diffusion coefficient for the full population. The dashed lines represent the expected two population distribution (see Supplementary Material for fit parameters). Histogram of diffusion coefficients for Tritc-DHPE at normal total cell cholesterol concentration (A) and after 2 h β -CD (B). Histogram of diffusion coefficients for Tritc-DHPE in the presence of TNBS at normal total cell cholesterol concentration (C) and after 2 h β -CD (D). DiIC₁₈ at normal total cell cholesterol concentration (E) and after 2 h β -CD (F). DiIC₁₈ with TNBS at normal total cell cholesterol concentration (G) and after 2 h β -CD (H).

After a 2 h β -CD treatment, the tubulin network was disrupted with nocodazole and the cells were imaged with the drug present in the media at 37°C. Treatment of the cholesterol-depleted cells with nocodazole also did not restore the mobility of the GPI-linked I-E^k (Fig. 6 C) or transmembrane I-E^k (Fig. 6 D), but instead caused a slight decrease in the diffusion coefficient (Table 1).

Temperature dependence of the diffusion coefficients at various cholesterol concentrations

The temperature dependence of the mean diffusion coefficients for GPI-linked and transmembrane I-E^k was investigated at normal and reduced cholesterol concentrations (Fig. 7, A and B). Arrhenius plots of these data were used to determine the activation energy for diffusion, E_a , using the relationship: $\ln(D) = \ln(D_0) - (E_a/RT)$, where $R = 8.314 \text{ Jmol}^{-1}\text{K}^{-1}$ (53–55). For normal cholesterol concentrations, the E_a for diffusion has a constant value for GPI-linked and transmembrane I-E^k over the temperature range of 22°C–42°C (Table 2). When the total cell cholesterol is reduced, the E_a changes at $\sim 35^\circ\text{C}$ for both proteins, thus suggesting a change in the phase behavior of the membrane at this temperature (Table 2). The change in the E_a value is observed when the cholesterol is depleted using either a 10 min or a 2 h β -CD treatment. The break in the Arrhenius plots was estimated to occur at $\sim 34^\circ\text{C}$ for the GPI-linked I-E^k after 2 h β -CD, $\sim 36^\circ\text{C}$ for the transmembrane I-E^k after 10 min β -CD, and $\sim 36^\circ\text{C}$ for the transmembrane I-E^k after 2 h β -CD.

DISCUSSION

No evidence of confinement was observed for any of the proteins or lipid analogs employed in our diffusion studies given a 15 ms integration time and ~ 0.5 s Cy5 on-time before photobleaching of the fluorophore. However, the diffusion of probes in the outer and inner leaflets of the plasma membrane responded differently to cholesterol depletion.

Several membrane molecules exhibited a decrease in their diffusion coefficients upon cholesterol extraction. These included the GPI-linked and transmembrane I-E^k proteins with large extracellular domains as well as the slow Tritc-DHPE population. Diffusion of probes located in the inner leaflet, the DiIC₁₈ and fast Tritc-DHPE population, were unaffected by cholesterol depletion. From Arrhenius plots of diffusion coefficient, we conclude that solid-like regions form in the outer leaflet of the plasma membrane and suppress diffusion of membrane molecules that are at least partially located in the outer leaflet.

Diffusion of I-E^k proteins is unconstrained and homogeneous

Diffusion coefficients from both the GPI-linked and transmembrane I-E^k proteins show homogeneous diffusion at all cholesterol concentrations when imaged at 37°C, indicating that the entire population of each protein diffuses in a similar environment regardless of the cholesterol concentration.

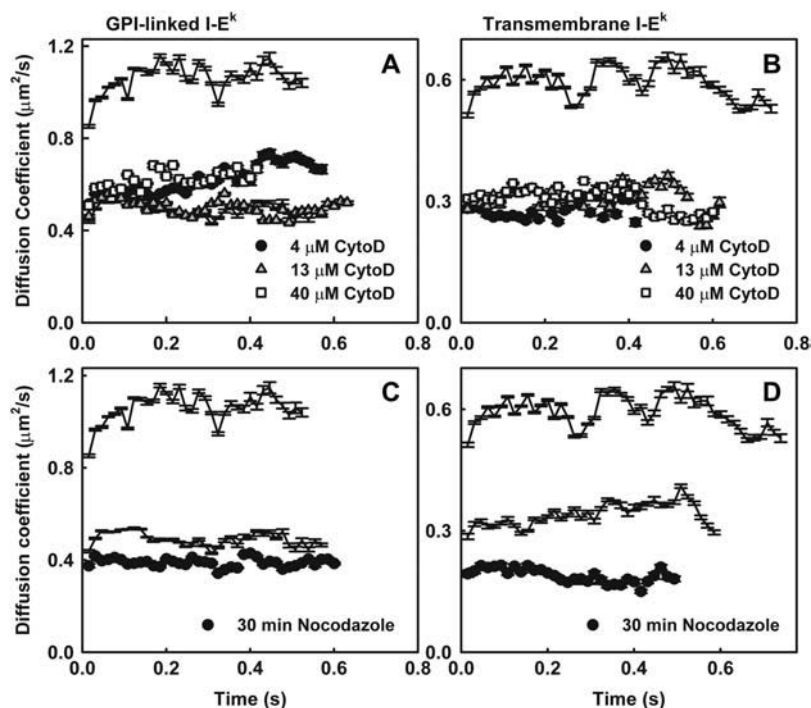


FIGURE 6 Effect of cytoskeletal disruption after cholesterol depletion at 37°C. Cells were pretreated with 2 h β -CD, then either the actin cytoskeleton was disrupted using 4, 13, or 40 μM cytochalasin D treatment (A and B) or microtubules were disrupted using nocodazole (C and D). (A) Diffusion coefficients as a function of time lag for GPI-linked I-E^k after actin cytoskeleton disruption. The D values at normal cholesterol ($D = 1.1 \pm 0.06 \mu\text{m}^2/\text{s}$) and after 2 h β -CD ($D = 0.49 \pm 0.03 \mu\text{m}^2/\text{s}$) are shown for comparison (lines with error bars). (B) D values as a function of time lag for transmembrane I-E^k after actin cytoskeleton disruption. The D values at normal cholesterol ($D = 0.59 \pm 0.04 \mu\text{m}^2/\text{s}$) and after 2 h β -CD ($D = 0.34 \pm 0.03 \mu\text{m}^2/\text{s}$) are shown for comparison (lines with error bars). (C) D values for GPI-linked I-E^k at 37°C after the tubulin network was disrupted. The D values at normal cholesterol and after 2 h β -CD are again shown for comparison (lines with error bars). (D) D values for transmembrane I-E^k at 37°C after the tubulin network was disrupted. The D values at normal cholesterol and after 2 h β -CD are again shown for comparison (lines with error bars).

Also, positional trajectories showed no evidence of confinement for GPI-linked or transmembrane I-E^k at any cholesterol concentration studied, for cells imaged at either room temperature (25,26) or 37°C. The diffusion for both proteins is predominately Brownian for the length of the trajectories at all studied cholesterol concentrations, as judged by our measured α -parameter, although instances of non-Brownian motion were observed for portions of single-molecule trajectories in very rare cases (~1%) (data not shown). The average on-time for a Cy5 molecule (0.5 s) and the integration time of one frame (15.4 ms) can be used to place bounds on the region of free diffusion. Given the diffusion coefficient at normal and ~50% normal total cholesterol, we observe unconstrained diffusion of the GPI-linked I-E^k protein in areas up to 2.2 μm^2 at normal or 1.0 μm^2 at ~50% normal total cell cholesterol. We observe unconstrained

diffusion in areas of up to 1.2 μm^2 at normal or 0.9 μm^2 at ~50% normal total cell cholesterol for transmembrane I-E^k protein ($\langle r^2 \rangle = 4Dt$). Using a more conservative estimate of the time required for a molecule to sense the confinement boundary for a stationary, impermeable domain ($\langle r^2(\infty) \rangle = Dt/4$) (56), the upper limit is 1.4 μm^2 at normal or 0.06 μm^2 at ~50% normal total cell cholesterol for GPI-linked I-E^k and 0.08 μm^2 or 0.05 μm^2 for transmembrane I-E^k. Our results do not preclude the existence of larger domains, mobile domains, domains with permeable boundaries, or dynamic domains.

At 37°C, the diffusion coefficients for the GPI-linked and transmembrane I-E^k proteins are cholesterol dependent, decreasing by a factor of 2.2 and 1.7, respectively, when the total cell cholesterol is reduced to ~50% of normal. The twofold decrease is similar to the magnitude of the decrease

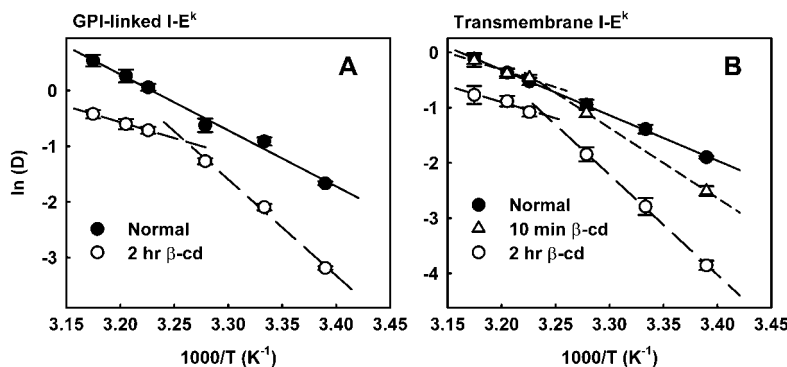


FIGURE 7 Arrhenius plot of the diffusion coefficients for the MHC proteins. Data were taken at temperatures between 22°C and 42°C. Normal refers to normal cholesterol concentration. (A) GPI-linked I-E^k. (B) Transmembrane I-E^k. Activation energies are reported in Table 2. Diffusion coefficients were calculated from fits to the cumulative distribution function averaged over all time lags. The number of tracks used in each case is reported in the Supplementary Material.

TABLE 2 Activation energies

E_a (kJ/mol)	GPI-linked I-E ^k		Transmembrane I-E ^k	
	(22°C–42°C)	(37°C–42°C)	(22°C–42°C)	(37°C–42°C)
Normal cholesterol	83.7 ± 4.4		68.4 ± 0.82	
2 h β-CD	143.6 ± 10.2	47.6 ± 1.1	150.5 ± 3.6	48.7 ± 13.4
10 min β-CD			106	52.0 ± 8.5

in diffusion coefficients reported by Kenworthy et al. (38) for GPI-linked and transmembrane proteins imaged in cells with ~30% of normal cholesterol levels at 37°C.

Heterogeneity in the diffusion of fluorescent lipid analogs

The distributions of diffusion coefficients for Tritc-DHPE at normal and reduced cholesterol concentrations were heterogeneous. At 22°C, there are two populations of diffusers with average values centered at ~2 and 0.2 μm²/s. Histograms of the diffusion coefficients for Tritc-DHPE show 80% of the population contributing to the slower diffusion coefficient. In the presence of TNBS, which quenches fluorophores in the outer leaflet, the relative size of the slower population is reduced by 25%, indicating that Tritc-DHPE in the slower population were present in the outer leaflet. The diffusion of Tritc-DHPE in the outer leaflet decreased ~6-fold after cholesterol depletion, whereas diffusion in the inner leaflet did not significantly change. Distributions of diffusion coefficients for DiIC₁₈ were homogeneous, and not significantly altered by the presence of TNBS. It is unlikely that all of the DiIC₁₈ is present in the inner leaflet. We speculate that the diffusion of DiIC₁₈ is similar in the inner and outer leaflets, and thus introduction of TNBS does not change the distribution of diffusion coefficients.

These results suggest that the regions in the inner leaflet probed by the fast Tritc-DHPE population and DiIC₁₈ respond differently to cholesterol depletion than the regions in the outer leaflet probed by the GPI-linked and transmembrane I-E^k proteins and the slower Tritc-DHPE population.

The composition of biological membranes is thought to be asymmetric; phosphatidylcholine and sphingomyelin lipids are enriched in the outer leaflet and lipids with phosphatidylethanolamine and phosphatidylserine headgroups are enriched in the inner leaflet (57). In erythrocyte plasma membranes, the inner leaflet is reported to contain more unsaturated lipids than the outer leaflet (58,59). The diffusion of fluorescent lipid analogs in the inner leaflet is reportedly faster than in the outer leaflet of the plasma membrane of human erythrocytes (60), Chinese hamster lung fibroblasts (61), and bovine aortic endothelial cells (62). The half-time of transbilayer diffusion for cholesterol in erythrocytes has been reported to range from <1 s (63) at 37°C to minutes at 4°C (64,65), so it is likely that cholesterol may redistribute between the two leaflets during the 2 h of β-CD treatment utilized here.

Temperature dependence of diffusion at reduced cholesterol concentrations suggests formation of solid-like regions

Arrhenius plots were used to analyze the temperature dependence of the mean diffusion coefficients for GPI-linked and transmembrane I-E^k proteins at different cholesterol concentrations in the range of 22°C to 42°C. At normal cell cholesterol concentration, the Arrhenius plots of the diffusion coefficients for both proteins are linear as the temperature of the cells is raised from room temperature to above physiological temperature (22°C–42°C). The activation energies (E_a) for diffusion for the I-E^k proteins are higher than the values of 12.6–54.4 kJ/mol reported for fluorescent lipid analogs with chain lengths from C6 to C18 diffusing in liquid multibilayers composed of dimyristoylphosphatidylcholine (DMPC), dioleoylphosphatidylcholine (DOPC), egg phosphatidylcholine, or bovine brain phosphatidylserine over a similar temperature range (53,54,66).

When the cell cholesterol was incrementally reduced, E_a gradually increased over the temperature range of from 22°C to ~35°C. After a 2 h β-CD treatment, the E_a values for the I-E^k proteins were similar to the E_a of 151 kJ/mol reported for NBD-PE diffusion in the gel phase of a DMPC multibilayer (55). Above ~35°C after cholesterol depletion, the E_a values for the diffusion of both the I-E^k proteins were similar to those reported for fluorescent lipid analogs (53,54,66). The change in E_a at ~35°C, for the proteins after cholesterol depletion, is consistent with a pseudo “phase transition” for the plasma membrane lipids.

In a previous work, we proposed that the observed decrease in the diffusion coefficients after cholesterol depletion at room temperature could be understood in terms of the model of condensed complexes in which cholesterol associates with high melting phospholipids to form a liquid (26). Removal of cholesterol then releases the high melting lipids from complexes to form a solid-like phase. These solid-like regions act as obstacles to diffusion. The constant E_a for diffusion at normal cell cholesterol and the subsequent increases in the observed E_a after cholesterol depletion support the model of solid-like domain formation in the plasma membrane caused by freezing of high melting phospholipids when cholesterol is removed. It is interesting to note that the biochemical and physical properties of fatty acid auxotrophs of *Escherichia coli* also display breaks in Arrhenius plots near the growth temperatures (67,68).

Cholesterol extraction affected various membrane probes to different extents. The diffusion coefficient of ~80–90% of the Tritc-DHPE molecules (the slow fraction) decreased by a factor of ~6 at 22°C and ~3 for the full population at 37°C when the cell cholesterol was reduced to ~50% of normal. However, the diffusion coefficient for ~10–20% of the Tritc-DHPE molecules (the fast fraction) was unaffected by cholesterol depletion over this range at both temperatures. In contrast, the DiIC₁₈ probe showed only a small drop in

diffusion upon cholesterol depletion. Taken together, the differences in cholesterol dependence for the GPI-linked and transmembrane I-E^k proteins, Tritc-DHPE, and DiIC₁₂ (26) or DiIC₁₈ indicate the presence of regional heterogeneity in the CHO cell plasma membrane and the differences in the region of the membrane sensed by the different probes. The effective viscosity of the membrane does not appear to have increased homogeneously after cholesterol depletion.

The decrease in the diffusion coefficients for the GPI-linked and transmembrane I-E^k could be ascribed to an increase in either the size of the diffusing object or the concentration or size of immobile obstacles present in the plasma membrane (45,69,70). The size of the diffusing object would need to increase to several microns in diameter to account for the observed decrease in the diffusion coefficient for the I-E^k proteins at room temperature (26). Alternately, the shape of the putative solid-like regions could be filamentous, thus suppressing the mobility of certain membrane molecules. However, no evidence of clustering or spatial heterogeneity has been observed for the GPI-linked I-E^k, transmembrane I-E^k, or Tritc-DHPE before or after cholesterol depletion in the fluorescence microscope images (data not shown). Certainly the heterogeneity in the Tritc-DHPE motion suggests that some of the lipid probes are in a more restricted environment than others. Nevertheless, we cannot make a definitive statement as to the shape of these solid-like regions, which appear to act as obstacles to the diffusion of certain molecules. The solid-like regions might be a solid solution, or glass. In the latter case the breaks in Arrhenius plots could be regarded as a glass transition.

Cytoskeletal effects are negligible

The decrease in the diffusion coefficients of the MHC proteins does not appear to be mediated by cytoskeletal interactions since neither prevention of actin polymerization nor depolymerization of the tubulin network led to an increase in the diffusion of the proteins after cholesterol depletion when imaged at 15.4 ms per frame. This result is consistent with our previous work at room temperature (25).

In the literature, actin disruption using varying cytochalasin D treatments has been reported to have an effect on the diffusion of certain membrane molecules. Kwik et al. (35) reported that a 10 μM (5 $\mu\text{g/ml}$) cytochalasin D treatment for 30 min after cholesterol depletion to 50–60% of normal cell cholesterol led to an increase in the mobile fraction of the human leukocyte antigen (HLA) proteins. In the same report, a 4 μM (2 $\mu\text{g/ml}$) cytochalasin D treatment for 3 min at room temperature and 20 min at 31°C after cholesterol depletion was reported to decrease the number of HLA molecules confined by the cholesterol-dependent, PIP2-mediated, reorganization of cytoskeleton (35). Murase et al. (41) reported that a 13 μM cytochalasin D treatment for 5 min at 37°C resulted in a fourfold increase in the area of confinement for Cy3-labeled 1,2-dioleoyl-*sn*-glycero-3-phosphoethanol-

amine (DOPE). In this study, we found no change in the diffusion coefficient for the GPI-linked or transmembrane I-E^k proteins after treatment with various concentrations of cytochalasin D after cholesterol depletion.

CONCLUSIONS

In this work, a temperature increase from 22°C to 42°C showed faster diffusion of transmembrane and GPI-linked MHC II proteins and lipid analogs, and for the case with lowered cholesterol, a change in activation energy for the motion, suggesting a change in the phase behavior of the plasma membrane. Whereas analysis of the diffusion for MHC II proteins showed homogeneous behavior, Tritc-DHPE motion showed a clear presence of two populations, the slower of which became even slower in its diffusion upon cholesterol extraction. The slow population is likely to arise from Tritc-DHPE localized in the outer leaflet. The variations in behavior are likely due to the differing inner-outer leaflet localization of the lipid analogs and the MHC II proteins in the plasma membrane. Taken together, these results provide evidence for the presence of solid-like regions in the plasma membrane at reduced cholesterol levels.

SUPPLEMENTARY MATERIAL

An online supplement to this article can be found by visiting BJ Online at <http://www.biophysj.org>.

The authors thank Michael Edidin for suggesting the use of a membrane impermeable fluorescence quencher.

This work was supported in part by National Science Foundation grant No. MCB-0212503, U.S. Department of Energy grant No. DEFG02-04ER63777, and National Institutes of Health grant No. 1 P20 HG003638-01 (W.E.M.). H.M.McC. acknowledges support from the Dept. of Chemistry at Stanford University.

REFERENCES

1. Subramanian, S., and H. M. McConnell. 1987. Critical mixing in monolayer mixtures of phospholipid and cholesterol. *J. Phys. Chem.* 91:1715–1718.
2. Dietrich, C., L. A. Bagatolli, Z. N. Volovyk, N. L. Thompson, M. Levi, K. Jacobson, and E. Gratton. 2001. Lipid rafts reconstituted in model membranes. *Biophys. J.* 80:1417–1428.
3. Dietrich, C., Z. N. Volovyk, M. Levi, N. L. Thompson, and K. Jacobson. 2001. Partitioning of Thy-1, GM1, and cross-linked phospholipid analogs into lipid rafts reconstituted in supported model membrane monolayers. *Proc. Natl. Acad. Sci. USA.* 98:10642–10647.
4. Samsonov, A. V., I. Mihalyov, and F. S. Cohen. 2001. Characterization of cholesterol-sphingomyelin domains and their dynamics in bilayer membranes. *Biophys. J.* 81:1486–1500.
5. Veatch, S. L., and S. L. Keller. 2002. Organization in lipid membranes containing cholesterol. *Phys. Rev. Lett.* 89:2681011–2681014.
6. Veatch, S. L., and S. L. Keller. 2003. Separation of liquid phases in giant vesicles of ternary mixtures of phospholipids and cholesterol. *Biophys. J.* 85:3074–3083.

7. Bagatolli, L. A., and E. Gratton. 2000. Two photon fluorescence microscopy of coexisting lipid domains in giant unilamellar vesicles of binary phospholipid mixtures. *Biophys. J.* 78:290–305.
8. Korlach, J., P. Schuille, W. W. Webb, and G. W. Feigenson. 1999. Characterization of lipid bilayer phases by confocal microscopy and fluorescence correlation spectroscopy. *Proc. Natl. Acad. Sci. USA.* 96:8461–8466.
9. Feigenson, G. W., and J. T. Buboltz. 2001. Ternary phase diagram of dipalmitoyl-PC/dilauroyl-PC/cholesterol: nanoscopic domain formation driven by cholesterol. *Biophys. J.* 80:2775–2788.
10. Vist, M. R., and J. H. Davis. 1990. Phase equilibria of cholesterol/dipalmitoylphosphatidylcholine mixtures: 2H nuclear magnetic resonance and differential scanning calorimetry. *Biochemistry.* 29:451–464.
11. Veatch, S. L., I. V. Polozov, K. Gawrisch, and S. L. Keller. 2004. Liquid domains in vesicles investigated by NMR and fluorescence microscopy. *Biophys. J.* 86:2910–2922.
12. Radhakrishnan, A., and H. M. McConnell. 1999. Cholesterol-phospholipid complexes in membranes. *J. Am. Chem. Soc.* 121:486–487.
13. Radhakrishnan, A., and H. M. McConnell. 1999. Condensed complexes of cholesterol and phospholipids. *Biophys. J.* 77:1507–1517.
14. McConnell, H. 2005. Complexes in ternary cholesterol-phospholipid mixtures. *Biophys. J.* 88:L23–L25.
15. McConnell, H. M., and A. Radhakrishnan. 2003. Condensed complexes of cholesterol and phospholipids. *Biochim. Biophys. Acta.* 1610:159–173.
16. McConnell, H. M., and M. Vrljic. 2003. Liquid-liquid immiscibility in membranes. *Annu. Rev. Biophys. Biomol. Struct.* 32:469–492.
17. Keller, S. L., W. H. Pitcher III, W. H. Huestis, and H. M. McConnell. 1998. Red blood cell lipids form immiscible liquids. *Phys. Rev. Lett.* 81:5019–5022.
18. Simons, K., and E. Ikonen. 1997. Functional rafts in cell membranes. *Nature.* 387:569–572.
19. Brown, D. A., and J. K. Rose. 1992. Sorting of GPI-anchored proteins to glycolipid-enriched membrane subdomains during transport to the apical cell surface. *Cell.* 68:533–544.
20. Schroeder, R., E. London, and D. Brown. 1994. Interactions between saturated acyl chains confer detergent resistance on lipids and glycosylphosphatidylinositol (GPI)-anchored proteins: GPI-anchored proteins in liposomes and cells show similar behavior. *Proc. Natl. Acad. Sci. USA.* 91:12130–12134.
21. Brown, D. A., and E. London. 2000. Structure and function of sphingolipid- and cholesterol-rich membrane rafts. *J. Biol. Chem.* 275:17221–17224.
22. Heerklotz, H., H. Szadkowska, T. Anderson, and J. Seelig. 2003. The sensitivity of lipid domains to small perturbations demonstrated by the effect of triton. *J. Mol. Biol.* 329:793–799.
23. Harder, T., P. Scheiffele, P. Verkade, and K. Simons. 1998. Lipid domain structure of the plasma membrane revealed by patching of membrane components. *J. Cell Biol.* 141:929–942.
24. Mayor, S., K. G. Rothberg, and F. R. Maxfield. 1994. Sequestration of GPI-anchored proteins in caveolae triggered by cross-linking. *Science.* 264:1948–1951.
25. Vrljic, M., S. Y. Nishimura, S. Brasselet, W. E. Moerner, and H. M. McConnell. 2002. Translational diffusion of individual class II MHC membrane proteins in cells. *Biophys. J.* 83:2681–2692.
26. Vrljic, M., S. Y. Nishimura, W. E. Moerner, and H. M. McConnell. 2005. Cholesterol depletion suppresses the translational diffusion of class II major histocompatibility complex proteins in the plasma membrane. *Biophys. J.* 88:334–347.
27. Anderson, R. G. W., and K. Jacobson. 2002. A role for lipid shells in targeting proteins to caveolae, rafts and other lipid domains. *Science.* 296:1821–1825.
28. Hao, M., S. Mukherjee, and F. R. Maxfield. 2001. Cholesterol depletion induces large scale domain segregation in living cell membranes. *Proc. Natl. Acad. Sci. USA.* 98:13072–13077.
29. Lommerse, P. H. M., H. P. Spaink, and T. Schmidt. 2004. In vivo plasma membrane organization: results of biophysical approaches. *Biochim. Biophys. Acta.* 1664:119–131.
30. Eddidin, M. 2003. The state of lipid rafts: from model membranes to cells. *Annu. Rev. Biophys. Biomol. Struct.* 32:257–283.
31. Xavier, R., T. Brennan, Q. Li, C. McCormack, and B. Seed. 1998. Membrane compartmentation is required for efficient T cell activation. *Immunity.* 8:723–732.
32. Field, K., D. Holowka, and B. Baird. 1997. Compartmentalized activation of the high affinity immunoglobulin E receptor within membrane domains. *J. Biol. Chem.* 272:4276–4280.
33. Sheets, E. D., D. Holowka, and B. Baird. 1999. Critical role for cholesterol in Lyn-mediated tyrosine phosphorylation of FcεRI and their association with detergent-resistant membranes. *J. Cell Biol.* 145:877–887.
34. Vidalain, P. O., O. Azocar, C. Servet-Delprat, C. Rabourdin-Combe, D. Gerlier, and S. Manie. 2000. CD40 signaling in human dendritic cells is initiated within membrane rafts. *EMBO J.* 19:3304–3313.
35. Kwik, J., S. Boyle, D. Fooksman, L. Margolis, M. P. Sheetz, and M. Eddidin. 2003. Membrane cholesterol, lateral mobility, and the phosphatidylinositol 4,5-bisphosphate-dependent organization of cell actin. *Proc. Natl. Acad. Sci. USA.* 100:13964–13969.
36. Shvartsman, D. E., M. Kotler, R. D. Tall, M. G. Roth, and Y. I. Henis. 2003. Differently anchored influenza hemagglutinin mutants display distinct interaction dynamics with mutual rafts. *J. Cell Biol.* 163:879–888.
37. Sooksawate, T., and M. A. Simmonds. 2001. Effects of membrane cholesterol on the sensitivity of the GABA(A) receptor to GABA in acutely dissociated rat hippocampal neurones. *Neuropharmacology.* 40:178–184.
38. Kenworthy, A. K., B. J. Nichols, C. L. Rimmert, G. M. Hendrix, M. Kumar, J. Zimmerberg, and J. Lippincott-Schwartz. 2004. Dynamics of putative raft-associated proteins at the cell surface. *J. Cell Biol.* 165:735–746.
39. Bacia, K., D. Scherfeld, N. Kahya, and P. Schuille. 2004. Fluorescence correlation spectroscopy relates rafts in model and native membranes. *Biophys. J.* 87:1034–1043.
40. Wettstein, D. A., J. J. Boniface, P. A. Reay, H. Schild, and M. M. Davis. 1991. Expression of a class II major histocompatibility complex (MHC) heterodimer in a lipid-linked form with enhanced peptide/soluble MHC complex formation at low pH. *J. Exp. Med.* 174:219–228.
41. Murase, K., T. Fujiwara, Y. Umemura, K. Suzuki, R. Iino, H. Yamashita, M. Saito, H. Murakoshi, K. Ritchie, and A. Kusumi. 2004. Ultrafine membrane compartments for molecular diffusion as revealed by single molecule techniques. *Biophys. J.* 86:4075–4093.
42. Rotsch, C., and M. Radmacher. 2000. Drug-induced changes of cytoskeletal structure and mechanics in fibroblasts: an atomic microscopy study. *Biophys. J.* 78:520–535.
43. Huby, R. D. J., A. Weiss, and S. C. Ley. 1998. Nocodazole inhibits signal transduction by the T cell antigen receptor. *J. Biol. Chem.* 273:12024–12031.
44. Wakatsuki, T., B. Schwab, N. C. Thompson, and E. L. Elson. 2000. Effects of cytochalasin D and latrunculin B on mechanical properties of cells. *J. Cell Sci.* 114:1025–1036.
45. Saxton, M. J. 1994. Anomalous diffusion due to obstacles: a Monte Carlo study. *Biophys. J.* 66:394–401.
46. Smith, P. R., I. E. G. Morrison, K. M. Wilson, N. Fernandez, and R. J. Cherry. 1999. Anomalous diffusion of major histocompatibility complex class I molecules on HeLa cells determined by single particle tracking. *Biophys. J.* 76:3331–3344.
47. Feder, T. J., I. Brust-Mascher, J. P. Slattery, B. Baird, and W. W. Webb. 1996. Constrained diffusion of immobile fraction on cell surfaces: a new interpretation. *Biophys. J.* 70:2767–2773.
48. Qian, H., M. P. Sheetz, and E. L. Elson. 1991. Single particle tracking. Analysis of diffusion and flow in two-dimensional systems. *Biophys. J.* 60:910–921.

49. Schütz, G. J., H. Schindler, and T. Schmidt. 1997. Single-molecule microscopy on model membranes reveals anomalous diffusion. *Biophys. J.* 73:1073–1080.
50. Wolf, D. E. 1985. Determination of the sidedness of carbocyanine dye labeling of membranes. *Biochemistry.* 24:582–586.
51. Schwiegelshohn, B., J. F. Presley, M. Gorecki, T. Vogel, Y. A. Carpentier, F. R. Maxfield, and R. J. Deckelbaum. 1995. Effects of apoprotein E on intracellular metabolism of model triglyceride-rich particles are distinct from effects on cell particle uptake. *J. Biol. Chem.* 270:1761–1769.
52. Murakoshi, H., R. Iino, T. Kobayashi, T. Fujiwara, C. Ohshima, A. Yoshimura, and A. Kusumi. 2004. Single-molecule imaging analysis of Ras activation in living cells. *Proc. Natl. Acad. Sci. USA.* 101:7317–7322.
53. Tamm, L. K., and H. M. McConnell. 1985. Supported phospholipid bilayers. *Biophys. J.* 47:105–113.
54. Vaz, W. L., Z. I. Derzko, and K. A. Jacobson. 1982. Photobleaching measurements of the lateral diffusion of lipids and proteins in artificial phospholipid bilayer membranes. In *Membrane Reconstitution*. G. Poste and G. L. Nicolson, editors. Elsevier Biomedical Press, Amsterdam. 83–136.
55. Smith, B. A., and H. M. McConnell. 1978. Determination of molecular motion in membranes using periodic pattern photobleaching. *Proc. Natl. Acad. Sci. USA.* 75:2759–2763.
56. Saxton, M. J. 1993. Lateral diffusion in an archipelago. Single-particle diffusion. *Biophys. J.* 64:1766–1780.
57. Devaux, P. F. 1992. Protein involvement in transmembrane lipid asymmetry. *Annu. Rev. Biophys. Biomol. Struct.* 21:417–439.
58. Myher, J. J., A. Kuksis, and S. Pind. 1989. Molecular species of glycerophospholipids and sphingomyelins of human erythrocytes improved methods of analysis. *Lipids.* 24:396–407.
59. Hullin, F., M.-J. Bossant, and N. Salem Jr. 1991. Aminophospholipid molecular species asymmetry in the human erythrocyte plasma membrane. *Biochim. Biophys. Acta.* 1061:15–25.
60. Morrot, G., S. Cribier, P. F. Devaux, D. Geldwerth, J. Davoust, J. F. Bureau, P. Fellmann, P. Herve, and B. Frilley. 1986. Asymmetric lateral mobility of phospholipids in the human erythrocyte membrane. *Proc. Natl. Acad. Sci. USA.* 83:6863–6867.
61. Chahine, J., S. Cribier, and P. Devaux. 1993. Phospholipid transmembrane domains and lateral diffusion in fibroblasts. *Proc. Natl. Acad. Sci. USA.* 90:447–451.
62. Julien, M., J.-F. Tournier, and J.-F. Tocanne. 1993. Differences in the transbilayer and lateral motions of fluorescent analogs of phosphatidylcholine and phosphatidylethanolamine in the apical plasma membrane of bovine aortic endothelial cells. *Exp. Cell Res.* 208:387–397.
63. Steck, T. L., J. Ye, and Y. Lange. 2002. Probing red cell membrane cholesterol movement with cyclodextrin. *Biophys. J.* 83:2118–2125.
64. Schroeder, F., G. Nemezc, W. Gibson Wood, C. Joiner, G. Morrot, M. Ayrault-Jarrier, and P. F. Devaux. 1991. Transmembrane distribution of sterol in the human erythrocyte. *Biochim. Biophys. Acta.* 1066:183–192.
65. Muller, P., and A. Herrmann. 2002. Rapid transbilayer movement of spin-labeled steroids in human erythrocytes and in liposomes. *Biophys. J.* 82:1418–1428.
66. Derzko, Z. I., and K. A. Jacobson. 1980. Comparative lateral diffusion of fluorescent lipid analogues in phospholipid multibilayers. *Biochemistry.* 19:6050–6057.
67. Tsukagoshi, N., and C. F. Fox. 1973. Transport system assembly and the mobility of membrane lipids in *Escherichia coli*. *Biochemistry.* 12:2822–2829.
68. Linden, C. D., K. L. Wright, H. M. McConnell, and C. F. Fox. 1973. Lateral phase separations in membrane lipids and the mechanism of sugar transport in *Escherichia coli*. *Proc. Natl. Acad. Sci. USA.* 70:2271–2275.
69. Saffman, P. G., and M. Delbruck. 1975. Brownian motion in biological membranes. *Proc. Natl. Acad. Sci. USA.* 72:3111–3113.
70. Hughes, B. D., B. A. Pailthorpe, and L. R. White. 1981. The translational and rotational drag on a cylinder moving in a membrane. *J. Fluid Mech.* 110:349–372.